# An Integrated View of Nonlinear Distortion Phenomena in Various Power Amplifier Technologies

Pedro Miguel Cabral, Nuno Borges Carvalho and José Carlos Pedro
Instituto de Telecomunicações - Universidade de Aveiro, Aveiro, Portugal, +351 234377900

*Abstract* - **This paper presents an integrated view of nonlinear distortion in various power amplifier, PA, technologies. Using very weak assumptions, it shows that large signal IMD sweet spots are inherent to a wide variety of PA technologies like Si MOSFET, Si LDMOS, Si BJT, GaAs MESFET, GaAs-AlGaAs HEMT, justifying their use in the design of highly linear and efficient PAs.**

## I. Introduction

RF power amplifiers, PAs, are the last active blocks in any wireless transmitter system, handling the highest levels of RF signal and supply power. Linearization enforcing techniques relying on either adding external circuitry to the PA, or simply improving its design [1], are thus necessary. However, since the first set of methods - known as external linearization [2] - involves several drawbacks like cost, size, effective bandwidth or difficulty of adjustment, there has been a growing interest in directly optimizing the actual PA linearity.

One possible way to achieve this design goal is to rely on certain bias points and power operating conditions, the so-called large signal IMD sweet-spots, which lead to improved carrier to IMD ratios (IMR) near the zones where power added efficiency is maximized [3-5]. In an IMD versus input power level, *Pin*, plot, they can take many forms from a barely noticeable decrease in the IMD slope to mild IMD valleys, or even sharp deeps in the IMD characteristic.

The first aim of this paper is to show that these large signal IMD sweet spots are not particular to a specific transistor or PA topology, but are inherent to a large variety of PA circuits and active device technologies like Si CMOS, Si LDMOS, Si BJT, GaAs MESFET and GaAs-AlGaAs HEMT. Therefore, it is shown that they constitute a reliable means of PA linearization.

As practical illustrations, the experimental existence of large signal IMD sweet spots in Si CMOS and GaAs MESFET based PAs are shown and discussed.

## II. Large Signal IMD Sweet Spots Study Revisited

Since a general description of large signal IMD sweet spots is yet unavailable, we have to rely on analytical solutions of approximated models, afterwards complemented by full numerical harmonic balance simulations. For that, the first simplification consists in transforming the bi-dimensional dependence of the active device output current, $i_O(t)$, on the input and output control voltages, $v_I(t)$ and $v_O(t)$, into an one-dimensional model, generating this way an equivalent transfer function, TF, $i_O[v_I(t)]$. This assumes a determined output boundary condition imposed by load impedance, $Z_L(\omega)$, $z_L(\tau)$:

$$v_O(t) = V_{DC} - \int_{-\infty}^{\infty} z_L(\tau)\, i_O(t-\tau)\, d\tau \tag{1}$$

where $V_{DC}$ is the applied output quiescent voltage; and the knowledge of the active device nonlinear model $i_O[v_I(t), v_O(t)]$. In order to guarantee general application of the following theory, the active device nonlinear model will only be framed by very weak assumptions. The first one is that its turn-on can be described by an exponential of input voltage. That is obviously true for bipolar devices, but is also commonly adopted to represent sub-threshold conduction in FETs as channel current is also determined by carrier diffusion [6]. Then, for increasing $v_I$ ($v_{GS}$) voltages, it is assumed that the FET passes through a nearly quadratic zone, which, due to short-channel effects [6], tends to become linear for even higher $v_{GS}$. Actually, it is this $i_{DS}(v_{GS})$ behaviour that is responsible for the typical sigmoid form of their transconductance $G_m(v_{GS})$, which was shown to be well reproduced by the following empirical expression [4]:

$$i_{DS}(v_{GS}) = \beta \frac{[smt(v_{GS})]^2}{1 + \theta\, smt(v_{GS})} \tag{2a}$$

where $smt(v_{GS})$ is a smooth turn-on function of $v_{GS}$ given by:

$$smt(v_{GS}) = K_V \ln\left(1 + e^{\frac{v_{GS}}{K_V}}\right) \tag{2b}$$

and $\beta$, $\theta$ and $K_V$ are empirical scaling parameters.

In bipolar devices we would expect a completely different $i_C(v_{BE})$ behaviour, as this relation is, to first order, always exponential. However, that is not the case in real amplifiers. In fact, if we take into account that, contrary to FETs, the transistor is not an open circuit when seen from the input, but draws an exponential base current, there will be another input boundary condition determining that:

$$v_{BE}(t) = v_I(t) - R_I \cdot i_B(t) \tag{3}$$

where $R_I$ is the internal source resistance. So, since output current, $i_C$, will be almost proportional of $i_B$, it will be described in implicit form as:

$$i_C(v_I) = I_S\, e^{\left(\frac{v_I - R_I . i_C / B_F}{\eta V_T}\right)} \tag{4}$$

whose correspondent transconductance is again a sigmoid [1].

If we now take the output boundary into account, $i_O(v_I)$ will be almost unchanged unless $v_I$ is so high that $R_L.i_O$ becomes close to $V_{DC}$ in (1). There, $v_O$ is so small that the FET enters the triode region and the bipolar enters saturation. $v_I$ rapidly looses control over $i_O$ and the TF saturates (the PA enters in strong compression).

The resemblance between the TF curves originated from FETs or BJT devices is so evident that they can be approximated by a global equivalent model or by the same first order piece-wise approximation. These are shown in Fig. 1.

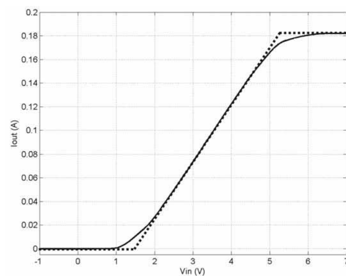


Fig. 1 Typical TF of a FET or bipolar active device '-' and its piece-wise approximation '--'.

Because IMD performance (as well as PA efficiency) varies dramatically with PA operation class, which is traditionally based in a conduction angle concept, hard to define from a real analytic TF, we need to start our discussion refining the classical definition of PA operation class.

In the piece-wise TF, the cut-off voltage defines the conduction angle, $2\theta$, which expresses the amount of time the device is on. So, if $2\theta < 180^{o}$ the amplifier is said to be in class C, if $2\theta = 180^{o}$ it is in class B, if $180^{o} < 2\theta < 360^{o}$ in class AB, and if $2\theta = 360^{o}$ the PA is said to operate in class A.

The main problem with this approach is the imprecise determination of cut-off voltage - since there is no clear break point – which then leads to ambiguous classification of PA operation. However, as we shall see in the following, if this zero order $i_O(v_I)$ based definition, is substituted by one based on higher order distortion effects, everything becomes more clear and consistent.

In order to do so, we shall look into the output 3rd harmonic content (for a sinusoidal excitation), where it is possible to see that the small signal 3rd harmonic (which is related to the 3rd order IMD and gain compression or expansion), changes with bias point, not only in amplitude, but also in phase (the sign in our memoryless nonlinearity), Fig. 2.

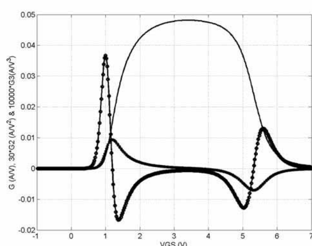


Fig. 2 First three coefficients of the TF Taylor series expansion: $G$ - '-', $G_2$ - 'x' and $G_3$ - 'o'.

From the 3rd derivative plot, we can find a null in the output 3rd derivative near the possible cut-off voltage. So, if the PA were biased at that point, there would be a null in the output 3rd harmonic. This result is exactly the one obtained if we bias the PA exactly at the break point of the piece-wise approximation, resulting in the so-called linear (for odd order distortion) class B PA. This observation allows a precise definition of a generalized cut-off voltage, and thus of PA operation class.

We can now re-state the definition of PA classes of operation relating them to that $G_3$ null. Class C is now a PA biased below that point, a class B is a PA biased exactly at the null, and classes A and AB correspond to PAs biased above that point.

This refinement of PA operation class is still consistent with every other property of the circuit, as it is shown in Fig. 3. As a matter of fact, this figure presents a comparison between main PA characteristics, of DC power consumption, output fundamental power and 2nd and 3rd harmonic content, obtained from three PA active device approximations: a FET based PA, a BJT based PA and the ideal piece-wise model [1]. The similarity of the three curve families is obvious.

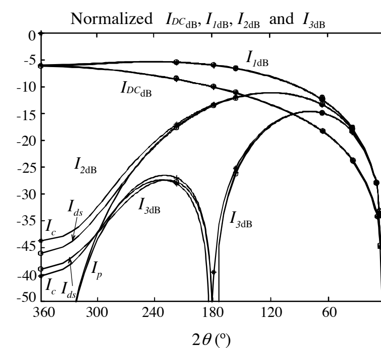


Fig. 3 Comparison of FET, BJT and piece-wise models.

With the PA operation class this way precisely defined, we can now focus on the large signal IMD sweet spots. They are critical points of IMD versus *Pin* characteristic, and can be interpreted as interactions between contributions of various orders of nonlinear distortion. So, it is convenient to begin studying small and large signal IMD separately.

Starting with small signal IMD analysis, we will use a low order Volterra series - or its memoryless subset, the Taylor series - of the output current of an active device:

$$I_{out}[v_{in}(t)] = I_{out\ DC} + G \cdot v_{in}(t) + G_2 \cdot v_{in}(t)^2 + G_3 \cdot v_{in}(t)^3 + \ldots \quad (5)$$

Fig. 2 presents the variation of these three small signal coefficients with bias point for a real active device.

Under large signal operation, the nonlinear response can be approximated by a sinusoidal or two-tone, $\omega_1$ and $\omega_2$, input describing function [3] which can be further simplified if a parabolic piecewise approximation is adopted to approximate the TF [5]. In addition, PA energy balance considerations have shown that the large signal asymptotic value of the IMD sidebands at $2\omega_1$-$\omega_2$ and $2\omega_2$-$\omega_1$ tend to a constant value of 180° phase [3].

Associating small and large signal IMD regimes, some important conclusions can be drawn:

1. Since small signal IMD phase is determined by the TF local derivatives, it can be directly controlled by changing the active device's bias point.

2. Since this TF is continuous and has a sigmoid shape, the IMD sidebands tend to a constant value with 180º phase (negative sign).

3. Since small signal IMD sign can be made positive (see Fig. 2), and tends to negative values in the large signal asymptote, the Bolzano-Weierstrass theorem guarantees the existence of at least one IMD null (a large signal IMD sweet spot) somewhere in between.

Given these general conclusions, and the above definitions, let us now study each operation class for a generic TF as the one presented in Fig. 1.

*A. Class C operation*

In this case, the small signal distortion can be calculated using Volterra Series, and it can be seen from (5) and Fig. 2, that the small signal IMD analysis presents a rise of 3dB/dB and has a 0º phase. Since in the large signal regime it must tend to a constant with 180º phase, then a minimum should appear in the transition between 0º and 180º phases.

*B. Class AB operation*

In class AB, the small signal IMD presents a phase of 180º and rises at 3dB/dB. In this case, the asymptotic behavior in large signal continues to be 180º and, at first sight, no large signal sweet spot would occur. Nevertheless, and depending on the difference between the contribution of the positive lobe of $G_3$, Fig. 2, and the negative one, it can be proved that a transition from 180º to 0º can occur at lower values of output power [4-5] generating an IMD sweet spot, and thus a new one will have to appear at large signal where 3rd order IMD tends again to 180º. So, in this case, and depending on the PA bias point, two sweet spots can be generated. Fager in [4-5] gives a further insight on the theoretical explanation of this behavior.

*C. Class A operation*

This class has a 3rd order IMD small signal 180º phase, and since it tends to an asymptotic value of 180º, no IMD sweet spot will be generated. In this case, and contrary to what was seen for class AB, no phase inversion is previewed, since the contribution from the negative lobe of $G_3$ is always much higher than the one of the positive lobe [3-5]. So, and unless the PA is biased above another small signal sweet spot found in certain MESFETs [7], no large signal IMD sweet spot will be seen.

## III. IMD Behavior for Different PA Technologies

In order to prove the ability of this analysis in describing IMD behavior in several PA technologies, various harmonic balance simulations for PAs biased at classes A, AB and C were performed. The models used were: BSIM3v3 [8] for Si MOS, Fager [4] for Si LDMOS, Pedro [9] for GaAs MES, Angelov [10] for GaAs-AlGaAs HEMT and the Gummel-Poon for the Si BJT [11].

*A. Si MOSFET*

From Fig. 4 it is possible to see that a large signal IMD sweet spot appears at class C, for high values of input power, while a double IMD sweet spot appears at class AB, and no sweet spot is visible in class A [5], as predicted.

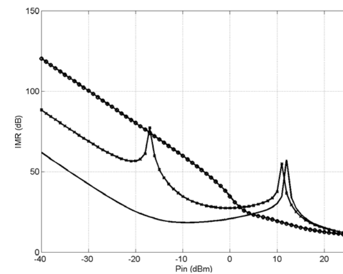


Fig. 4 IMR for a Si MOSFET PA at three operation classes: C - '-', AB - 'x' and A - 'o'.

IMR in class AB and class C is better than in class A for high values of input power. This fact, associated to the higher gain and power added efficiency of class AB, justifies its use in PAs of optimized linearity/efficiency.

*B. Si LDMOS*

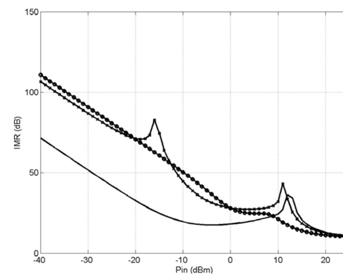


Fig. 5 IMR for a Si LDMOS PA at three operation classes: C - '-', AB - 'x' and A - 'o'.

As depicted in Fig. 5, LDMOS presents similar results to the ones already studied for CMOS [4].

*C. GaAs MESFET*

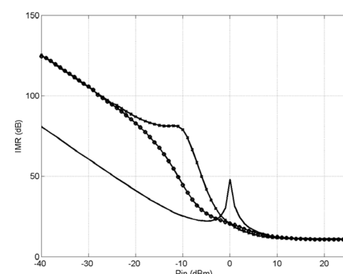


Fig. 6 IMR for a GaAs MESFET PA at three operation classes: C - '-', AB - 'x' and A - 'o'.

Fig. 6 presents the results obtained for MESFET based PAs [3], in which IMR for classes A and C present the same aspect as seen before. However, class AB no longer presents two peaks, but a rather smoother one. That slight increase in IMR at medium signal level regime can be attributed to an interaction between the negative $G_3$ and the positive higher orders' contributions. Nevertheless, they are not strong enough to generate a phase change, and thus neither a strong IMR maximum at medium signal excursions is visible, nor there is any large signal IMD sweet spot.

*D. GaAs-AlGaAs HEMT*

Fig. 7 presents the results for a HEMT based PA. These plots are similar to the ones already obtained for CMOS and LDMOS. So, the conclusions are similar.

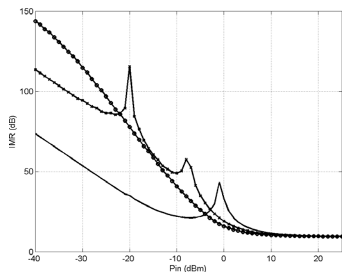


Fig. 7 IMR for a HEMT PA at three operation classes: C - '-', AB - 'x' and A - 'o'.

*E. Si BJT*

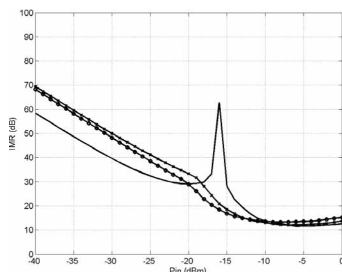


Fig. 8 IMR for a Si BJT PA at three operation classes: C - '-', AB - 'x' and A - 'o'.

As seen from Fig. 8, and predicted during the TF derivation, the results obtained for the BJT based PA are similar to the ones observed for the MESFET.

## IV. EXPERIMENTAL RESULTS

In order to provide experimental illustration of these simulated predictions Fig. 9 and Fig. 10 present measured results of two-tone IMD performance of a CMOS and MESFET based PAs in classes C, AB and A at 950 MHz and 2 GHz, respectively.

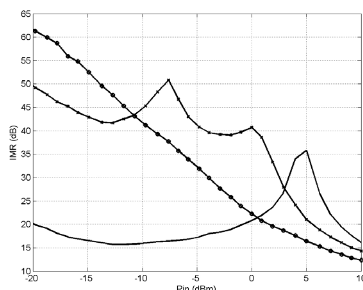


Fig. 9 Experimental IMR for a CMOS PA at three operation classes: C - '-', AB - 'x' and A - 'o'.

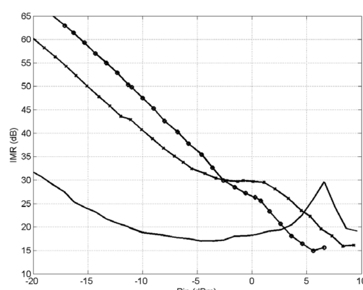


Fig. 10 Experimental IMR for a MESFET PA at three operation classes: C - '-', AB - 'x' and A - 'o'.

The experimental observations clearly support the simulated predictions shown in Figs. 4 and 6 for the corresponding PA technologies.

## V. CONCLUSIONS

In this paper a first integrated overview of distortion in different PA technologies was presented. It was seen that large signal IMD sweet spots are inherent to the physical device characteristics and that their appearance is related with PA classes of operation which were, therefore, more precisely defined.

## ACKNOWLEDGEMENTS

The authors would like to acknowledge Christian Fager and João Paulo Martins for their collaboration on the measurements; Portuguese Science Bureau, F.C.T., and the FEDER Program for financial support provided under Project POCTI/ESE/37531/2002 – OPAMS; and finally Portuguese Science Bureau, F.C.T., for the Ph.D. grant Ref. 11323/2002, given to the first author.

## REFERENCES

[1] J. C. Pedro and N. B. Carvalho, *Intermodulation Distortion in* Microwave *and Wireless Circuits*, Artech House, Norwood, 2003.

[2] P. B. Kennington, *High-Linearity RF Amplifier Design,* Artech House, Norwood, 2000.

[3] N. B. Carvalho and J. C. Pedro, "Large- and small-signal IMD behavior of microwave power amplifiers," *IEEE Trans. on Microwave Theory and Tech.*, vol. MTT-47, pp. 2364-74, Dec. 1999.

[4] C. Fager, J. C. Pedro, N. B. Carvalho, and H. Zirath, "Prediction of IMD in LDMOS transistor amplifiers using a new large-signal model," *IEEE Trans. on Microwave Theory and Tech.*, vol. MTT-50, pp. 2834-42, Dec. 2002.

[5] C. Fager, *Microwave FET Modeling and Applications*, Ph.D. Thesis, Chalmers University of Technology, 2003.

[6] Y. Tsividis, *Operation and Modeling of the MOS Transistor*, McGraw-Hill Int. Ed., 1988.

[7] J. C. Pedro and J. Perez, "Accurate Simulation of GaAs MESFET's Intermodulation Distortion Using a New Drain-Source Current Model", *IEEE Trans. on Microwave Theory and Tech.*, vol. MTT-42, pp. 25-33, Jan. 1994.

[8] Y. Cheng and C. Hu, *Mosfet Modeling & BSIM3 Users's Guide*, Kluwer Academic Pub., Boston, 1999.

[9] J. C. Pedro, "Physics Based MESFET Empirical Model", *1994 IEEE MTT-S Intern. Microwave Symposium Dig.*, pp.973-976, San Diego, 1994.

[10] I. Angelov, H. Zirath and N. Rorsman, "A New Empirical Nonlinear Model for HEMT and MESFET Devices", *IEEE Trans. on Microwave Theory and Tech.*, vol. MTT- 40, pp.2258-66, Dec. 1992.

[11] H. Gummel and H. Poon, "An Integral Charge Control Model of Bipolar Transistors," *Bell System Technical Journal*, vol. 49, no. 5, pp. 827, 1970.